THE JOURNAL OF PHYSICAL CHEMISTRY C

Article

pubs.acs.org/JPCC

Fast and Reliable Metamodeling of Complex Reaction Spaces Using Universal Kriging

Richard M. Maceiczyk and Andrew J. deMello*

Department of Chemistry and Applied Biosciences, Institute of Chemical and Bioengineering, ETH Zürich, Vladimir Prelog Weg 1, 8093 Zürich, Switzerland

Supporting Information

ABSTRACT: We report the application of metamodeling algorithms based on Universal Kriging for the controlled synthesis of compound semiconductor nanoparticles. Application of such a metamodel allows the prediction of reaction outcomes at arbitrary points within sparsely sampled parameter spaces as a function of reaction conditions. To demonstrate the applicability of Universal Kriging to chemical reaction screening within microfluidic reaction systems CdSe and CdSeTe quantum dots were synthesized by using a segmented flow capillary reactor. Variation of input reagent flows (to control reagent concentrations and reaction residence times) and online spectroscopic monitoring of product characteristics was achieved in a fully automated manner. The resulting fluorescence spectra are analyzed to extract the fwhm, wavelength maximum, and intensity of the band-edge emission. These values are subsequently used as inputs for the Universal Kriging metamodeling algorithm to predict the reactor output at arbitrary points within accessible parameter space. Results demonstrate that the algorithm can predict reaction outcomes with high accuracy and reliability.

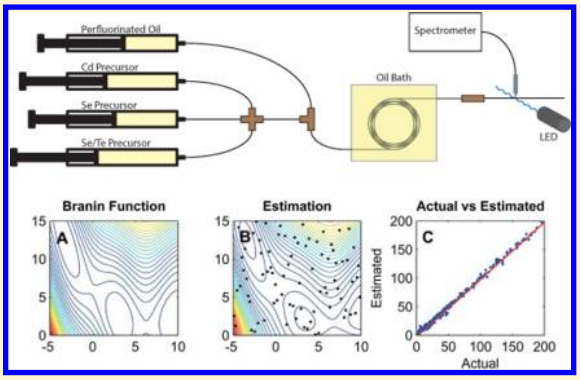

INTRODUCTION

Nanomaterials possess electronic and optical characteristics that typically differ greatly from the bulk materials from which they are derived.[1,2] This fact opens up opportunities for their use in a wide range of applications such as catalysis,[3] energy storage and generation,[4] photonics,[5] biosensing,[6] and medicine.[7] In particular, quantum dots, nanometer-sized semiconductor materials small enough to experience quantum confinement effects, possess band gaps that are a direct function of crystallite size thus allowing the production of particles with tunable emission over a wide range of energies.[8] The ability to precisely tune this band gap (and thus emission wavelength) requires strict control of reaction conditions such as temperature, precursor ratios, and reaction time during particle synthesis.[9] In recent years microfluidic reactors have been shown to provide for such control and are increasingly used to synthesize nanomaterials of defined chemical and physical properties.[10,11] To date microfluidic methods have been used to synthesize a range of nanomaterials including CdSe, CdS, InP, Ag, Au, Co, TiO_2, SiO_2, $LaPO_4$, $CaCO_3$, Fe_xO_y, zeolites, and $BaSO_4$, as well as more complicated core/shell structures such as CdSe/ZnS, Fe_2O_3/SiO_2, SiO_2/Au, Au/Ag/Au, and CdSe/ZnSe/ZnS.[12]

In simple terms, operation within microfluidic environments affords significant advantage in terms of heat and mass transfer, parameter control, and the ability to integrate real-time monitoring of the reaction products.[13] In contrast, flask-based synthetic methods[14] require extensive experimental effort to develop protocols that reproducibly lead to the production of high-quality quantum dot populations of defined size and size distribution. Indeed, it is well-recognized that the on-demand production of bespoke nanoparticles of arbitrary size remains a significant industrial challenge, with most quantum dots only commercially available in a small range of defined sizes.[15]

In theory, the adoption of microfluidic approaches alleviates this problem as hundreds of experiments can be carried out within hours by using minute amounts of reagent to find the precise experimental conditions that yield particle populations of the desired average size, size distribution, and fluorescence quantum efficiency.[10] Nevertheless, it is still undesirable to scan the entire set of conditions within accessible parameter space to ensure that reagent and time consumption are kept to a minimum, especially in complex multiparameter reaction systems. Accordingly, there is a defined need for the utilization of metamodeling techniques that are computationally fast, show high accuracy in their prediction of product parameters, and are easy to implement. To date a number of studies have reported the use of optimization routines to guide and accelerate the identification of optimal reaction conditions for the synthesis of predefined nanomaterials. Examples include artificial neural networks in the combinatorial synthesis of CdSe[16] and the use of noise-tolerant global search algorithms to find optimal conditions for the synthesis of CdSe quantum dots with

Received: June 24, 2014
Revised: August 8, 2014
Published: August 8, 2014

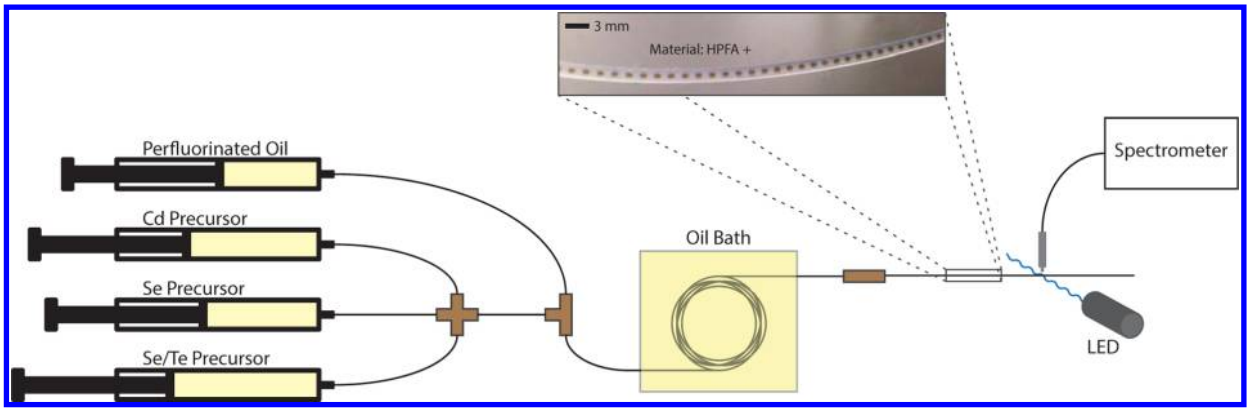

Figure 1. Schematic of the setup used for the microfluidic synthesis of quantum dots. The inset shows formed droplets containing CdSeTe quantum dots after leaving the oil bath.

predefined properties.[10] Despite their utility, the above-mentioned methods are either computationally intensive,[16] not model based (and thus do not allow accurate prediction of points between the samples),[17] or optimize an objective function, thereby obscuring the actual physical parameters of the products and potentially penalizing desirable products heavily due to arbitrarily chosen weighting coefficients.[10] Accordingly, there have been surprisingly few reports of using microfluidic reactors to make nanomaterials of predefined characteristics.[11,18] To directly address this issue we describe herein an automated microfluidic reaction system incorporating a metamodeling algorithm based on Universal Kriging that allows the prediction of product characteristics in regions of parameter space between sampled points. This approach provides a route to on-demand synthesis of high-quality, bespoke quantum dots of defined size. We show that the method outperforms literature methods in its computational efficiency and outstanding "intuition" in predicting product parameters even in scarcely sampled reaction systems.

An Automated Microfluidic Reactor for Quantum Dot Synthesis. Quantum dots (CdSe or CdSeTe) are synthesized in the microfluidic reactor depicted schematically in Figure 1. Details regarding this setup are elaborated in the Supporting Information. The Syringe pumps that deliver reagents to the reactor and the spectrometer are controlled by using in-house LabVIEW code. Two or three precursor streams for CdSe or CdSeTe synthesis, respectively, are united in a microfluidic mixer at different ratios. This stream is then segmented into nanoliter-volume droplets by a perfluorinated oil continuous phase. Segmentation significantly reduces problems[19] with reactor fouling,[20] eliminates residence time distributions,[21] and increases mixing efficiency due to a circulating flow profile[22] within each droplet. Particle nucleation and growth take place within a PTFE capillary immersed in an oil bath at a fixed temperature, with the reaction residence time being controlled by variation of the total flow rate of all inlet streams. After each change to a new set of parameters the reactor is left to stabilize for 2.5 residence times before the emission spectrum of the product particles is recorded. Reaction products are excited at 405 nm and emission spectra collected and processed with use of in-house MATLAB code to extract the emission maximum, full width at half-maximum (fwhm), and intensity of the band edge emission. A Universal Kriging metamodel is then fitted to the data to obtain an estimation for the entire parameter space.

Universal Kriging and Model Evaluation. Kriging is a statistical interpolation technique conceived by Daniel Krige to estimate the distribution of gold ores in samples obtained at bore holes at the Witwatersrand reef complex in South Africa and further developed by Georges Matheron.[23] It is a distance weighted interpolation method, meaning that samples closer to the point to be predicted have more influence on the prediction than those further away. Weighting coefficients are chosen in a way that ensures that the variance of the estimation is minimal. Excellent introductions to the Theory of Kriging can be found elsewhere.[24,25] Accordingly only a short introduction to the method will be given here. Data are presumed to originate from a Gaussian stochastic process $\{Z(s): s \in D\}$, where D is a fixed subset of a d-dimensional space from which samples are collected and used to perform inference on the process. This process is assumed to be *intrinsically stationary*, thus fulfilling

$$E(Z(s+h) - Z(s)) = 0 \tag{1}$$

$$\mathrm{Var}(Z(s+h) - Z(s)) = 2\gamma(h) \tag{2}$$

at any point s with $2\gamma(h)$ as *variogram*, which is a function of only h, an arbitrary distance. This means that the expected value of a measurement is uniform over the entire parameter space with the variance between two points a given distance apart given by the variogram. Some authors prefer to define a *covariogram* $C(h) = \mathrm{cov}(Z(0),Z(h))$ instead of the variogram. However, for a covariogram to exist the process $Z(s)$ must be covariance stationary (second order stationary), which is a stricter condition than intrinsic stationarity. Since the class of second order sationary processes is contained in the class of intrisic stationary processes, every existing covariogram can be converted to a variogram via the relation $2\gamma(h) = C(0) - C(h)$. This is why Kriging is defined here via the variogram. The variogram function is not known a priori but must be estimated from the data. The classical estimator[24] for the variogram is given by

$$2\hat{\gamma}(h) \equiv \frac{1}{|N(h)|} \sum_{N(h)} (Z(s_i) - Z(s_j))^2 \tag{3}$$

which is unbiased but not resistant to contamination (e.g., by systematic measurement error) in the data. Here $|N(h)|$ is the number of points that lie within a certain binning tolerance around the exact distance h. Since the value of the variogram is not known at every distance a model must be fitted to the empirical variogram. Possible shapes that a variogram can assume are shown in Figure 2. The process $Z(s)$ can be separated to yield

dx.doi.org/10.1021/jp506259k | J. Phys. Chem. C 2014, 118, 20026−20033

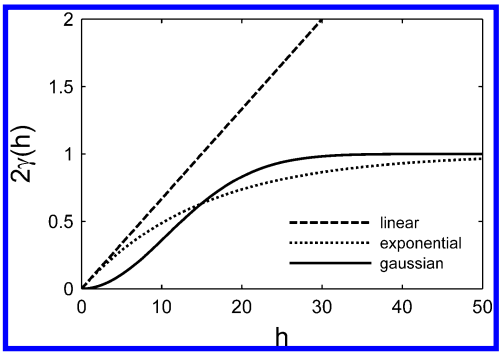

Figure 2. Examples for typical variogram models.

$$Z(s) = \mu + \delta(s) \tag{4}$$

where μ is a deterministic component, the mean, and $\delta(s)$ is a zero mean stochastic process fluctuating around μ. The three basic flavors of Kriging are distinguished through the behavior of μ. In *Simple Kriging* the mean is constant and known, in *Ordinary Kriging* the mean is constant but unknown, whereas in *Universal Kriging* (the method used in this work) the mean is unknown and a function of the spatial coordinates. In the case of Universal Kriging eq 4 can be rewritten as

$$Z(s) = \sum_{j=1}^{p} \beta_j f_j(s) + \delta(s) \tag{5}$$

The functions $f_j(s)$ define shape functions used to model the deterministic component and must be known. They can be obtained via linear regression and variance analysis or simply by exploratory data analysis.[25] Methods to estimate the validity of the chosen shape functions are discussed below. The coefficients β_j are calculated and therefore not needed a priori. For $p = 1$ and $f_1 = 1$ Ordinary Kriging is recovered. Now the linear, unbiased Universal Kriging estimator

$$\hat{Z}(s_0) = \sum_{i=1}^{N} \lambda_i Z(s_i) \tag{6}$$

for the point s_0 given N observations at the points $s_1 \ldots s_N$ can be obtained by minimizing its mean square prediction error under the constraint

$$\sum_{i=1}^{N} \lambda_i = 1 \tag{7}$$

using the method of Lagrange multipliers.[26] The obtained system of linear equations must then be solved for every point to be estimated. The variance of the prediction (Kriging variance) is obtained from

$$\sigma^2(s_0) = 2\sum_{i=1}^{n} \lambda_i \gamma(s_0 - s_i) - \sum_{i=1}^{n}\sum_{j=1}^{n} \lambda_i \lambda_j \gamma(s_i - s_j) \tag{8}$$

and can later be used to access the validity of the model as explained further below.

For Kriging, as well as for other metamodeling techniques, appropriate sampling is of high importance. Sampling schemes designed for low-order polynomial models typically used in traditional design of experiments (DOE) such as full- or fractional-factorial designs are not suitable. Instead, space-filling designs are required. A popular method is Latin hypercube sampling (LHS) originally invented for computer simulations.[27]

To construct a Latin hyper cube sampling scheme for N samples the parameter space is divided equally into N rows and N columns. The resulting cells are now sampled randomly but such that each row and column contains exactly one sample. This scheme can be extended accordingly to arbitrary dimensions. It is possible (but unlikely) that by chance most of the measurements lie on the main diagonal and are thus unsuitable for metamodel fitting due to the high correlation of the measurements. Different criteria have been suggested to optimize the properties of the LHS design. These include maximizing the minimum euclidean distance between measurements, minimizing the maximum euclidean distance between measurements or optimizing the orthogonality of the sampling points, thus reducing correlation; the latter being the criterion used in the present work.[28−30]

Kriging typically shows high accuracy in predicting even sparsely sampled parameter spaces.[31] In Figure 3 the performance of Ordinary Kriging with respect to the Branin test function (commonly used in optimization problems) is shown. Ordinary Kriging is appropriate in this situation (as opposed to Universal Kriging) since no trend in the original function can be identified. After only 80 sampled points chosen randomly in the fashion of a Latin square design, the true shape of the parent function is accurately reproduced by the metamodel. The estimated vs actual plot for 300 randomly chosen points throughout parameter space indicates high accuracy that is independent of the function value both in the middle and close to the borders of the sampled space.

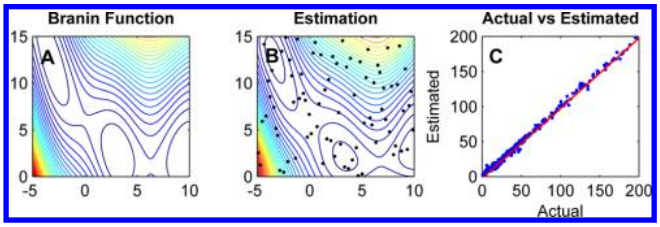

Figure 3. Branin function (A) shown together with the Ordinary Kriging estimation (B) after sampling at 80 randomly selected points indicated as black dots. The actual vs estimated plot (C) compares the actual function value with the value obtained via Kriging at 300 randomly selected points throughout parameter space.

A first impression of the quality of the fitted model can be obtained via visually inspecting the residuals.[25] Ideally there should be no visible patterns or trends and the residuals should be normally distributed around zero. Once the model has been deemed adequate via visual analysis of the randomness of the residuals more sophisticated methods can be used to confirm the validity of the chosen form of the shape functions. A popular method is *leave-one-out cross validation*.[32] Here each observation in the data set is removed one by one with the remaining observations then being used to obtain a prediction at the position s_i of the removed observation. The residual at that point is then divided by the Kriging standard deviation $(\sigma_{S_i}^2)^{1/2}$ calculated by using eq 8 to obtain the standardized residual r_i. There are two different ways of obtaining a prediction at each point. One is to use the variogram fitted using all observations including the one to be removed, the other is to remove the observation and fit a variogram model for every residual. Usually for larger samples the difference between the two methods is negligible and the single variogram method is used for simplicity. The standardized residuals

dx.doi.org/10.1021/jp506259k | J. Phys. Chem. C 2014, 118, 20026−20033

obtained via either method are then used to calculate these statistics:

$$S_1 = \frac{1}{N}\sum_{i=1}^{N} r_i \tag{9}$$

$$S_2 = \frac{1}{N}\sum_{i=1}^{N} r_i^2 \tag{10}$$

If the model is valid, S_1 should be close to zero and S_2 close to one. However, in reality it is very unlikely for them to take exactly these values since they are actually samples of variables with a mean of zero and one, respectively. Different methods have therefore been suggested to obtain better residuals.[33] However, the standard method is sufficient for the purpose of the current work since the validity of the model is assessed directly via experiment. For the computational example performed in Figure 3 S_1 = 0.04 and S_2 = 1.26 are extracted.

RESULTS AND DISCUSSION

Performance of the Microfluidic Reactor System. The quality of the quantum dots synthesized in the reactor is generally high. Synthesized nanoparticles show narrow band edge emission peaks with negligible defect emission. Due to the large body of characterization data available for CdSe and CdSeTe, not only from batch experiments but also for particles synthesized in reactors similar to the one presented here,[22,34] the emission spectra are deemed appropriate to evaluate the quality of these materials.

Figure 4 shows the stability of the capillary reactor equipped with a new capillary over a period of 8 h when synthesizing CdSe quantum dots at 220 °C with a 120 s residence time. Over the first 5 h the emission wavelength decreases about 7 nm and then remains approximately constant at 555 nm. Such a deviation is not large enough to introduce significant systematic error in the prediction since it is averaged out by virtue of the fact that samples are taken at random.

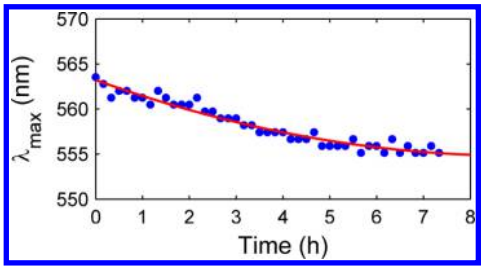

Figure 4. Stability of the microfluidic reactor over the course of 8 h when synthesizing CdSe quantum dots at 220 °C and a 120 s residence time. Measurements were taken every 10 min. The red line serves as a guide to the eye.

In the case of CdSe quantum dots the reactor could be operated for extended periods of time, as no fouling of the capillary was observed. Even larger particles synthesized at prolonged reaction times did not tend to aggregate and precipitate within the reactor. CdSeTe, however, proved very different. Larger CdSeTe quantum dots were often observed to aggregate and precipitate within the droplets, thus creating some reactor fouling. Accordingly the lifetime of the capillary was limited and was exchanged periodically, as explained further below.

Residence time and precursor flow ratio are key parameters in the synthesis of CdSe nanoparticles in flow.[21] In principle, temperature can also be used as an input parameter but the high film temperatures occurring during heat up lead to degradation of the silicon oil and solidification. Therefore, the temperature was kept constant. The precursor flow ratio is parametrized by defining

$$R = \frac{F_{Cd}}{F_{Cd} + F_{Se}}100 \tag{11}$$

where F_{Cd} and F_{Se} are inlet flow rates of the cadmium and selenium precursor streams, respectively. The direct ratio (F_{Cd}/F_{Se}) is not appropriate for Kriging since it presents a nonlinear functional dependence with respect to F_{Se} and a linear functional dependence with respect to F_{Cd}. In the case of CdSeTe synthesis an additional parameter is defined as

$$R' = \frac{F_{Se}}{F_{Te} + F_{Se}}100 \tag{12}$$

This accounts for the ratio of selenium to tellurium flow. The definition of R is altered to yield

$$R = \frac{F_{Cd}}{F_{Cd} + F_{Se} + F_{Te}}100 \tag{13}$$

This modification reflects the ratio of chalcogenide to cadmium precursor flow. Figure 5 shows the exemplary level of control over the reaction parameters that can be achieved by using the current system. With increasing temperature the particle

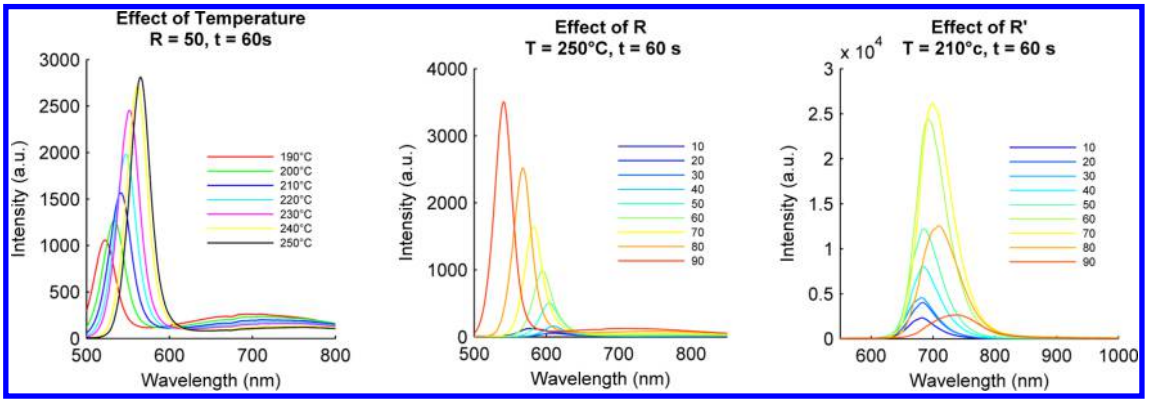

Figure 5. Effects on the photoluminescence of the synthesized quantum dots when varying T, R (CdSe), or R' (CdSeTe) with other parameters being kept constant.

dx.doi.org/10.1021/jp506259k | J. Phys. Chem. C 2014, 118, 20026−20033

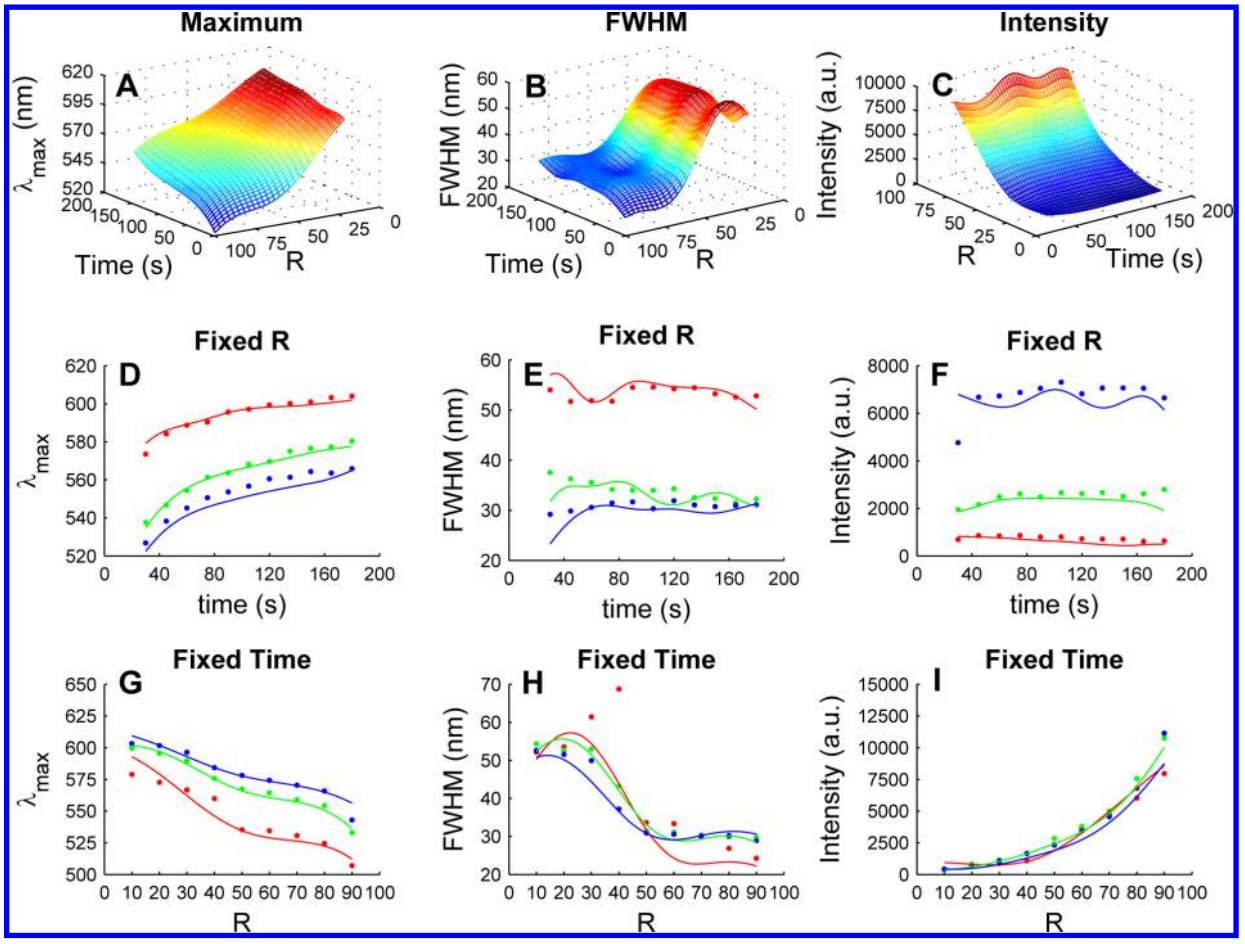

Figure 6. First row shows the obtained metamodels of maximum (A), fwhm (B), and intensity (C) for all parameter combinations within the chosen boundaries of time and R in the case of CdSe synthesis. Below each model the results of the validation experiment (see text) are shown. The solid lines represent the predictions with the metamodel whereas the dots correspond to measured values in the validation experiment. The measurements were taken at fixed R values (D, E ,F) of 20 (red), 50 (green), and 80 (blue) or at fixed reaction residence times (G, H, I) of 30 (red), 100 (green), and 180 s (blue).

growth is accelerated, leading to lower energy emission with higher intensity. The effect of varying R is more complex. The emission shifts to higher wavelengths as R is varied between 10 and 30 and then back to lower wavelengths as R is further increased. The intensity of luminescence initially decreases to a minimum value at R = 30 and then increases for R > 30. Varying R' and thus the chalcogenide ratio in the nanocrystals also leads to a nonlinear variation of the emission spectra, which agrees with previous bulk experiments.[35]

Prediction of Product Parameters for the Synthesis of CdSe. The Kriging metamodeling of the parameter space for the synthesis of CdSe in the reactor is a two-dimensional problem since only R, the parameter defining the precursor ratio, and the residence time t in the reactor are considered. The temperature is kept constant at 230 °C. To obtain the model, 80 parameter combinations where collected via a Latin square design. The residence time t was varied between 30 and 180 s and R between 10 and 90. The molar ratio of the Cd and Se precursor solutions is Se:Cd = 2:1. After prediction with Universal Kriging, the validity of the prediction was tested by sampling 11 points along lines of fixed R or t. The outcome of this experiment is shown in Figure 6. First it can be observed that the position of the emission maximum moves to lower energies with increasing time and decreasing R, thus indicating the formation of larger quantum dots. The fwhm remains around 30 nm for R values above 50 and then increases rapidly. The evaluation confirms the validty of the model with the only exception being data associated with t = 30 s, which lies on the border of the evaluated parameter space. Here the fwhm behaves in an irregular manner and the prediction only gives a trend estimation. The fluorescence intensity continuously increases as a function of R, but shows a much smaller dependence on time. For both emission maximum and intensity the evaluation experiments show that the accuracy of the prediction is of excellent quality. In this case the models show that the ratio of Se:Cd of 2:1 (R = 50) represents a good compromise between low fwhm and high intensity.

Prediction of Product Parameters for the Synthesis of CdSeTe. The evaluation of parameter space for the synthesis of CdSeTe nanoparticles in the reactor provides a more significant challenge than in the case of CdSe, not only because of the added dimension when introducing R', but also because of a more complicated chemistry involved. TeTOP (TOP: trioctylphosphine) is more reactive than SeTOP thus making direct predictions of the composition of product particles from the precursor ratio difficult. Furthermore, the bandgap is a nonlinear function of the Se:Te ratio in the final particle. It has its lowest energy at a Te content of about 60%.[36] Due to the high reactivity of TeTOP the precursor solution was mixed 1:1 with SeTOP precursor thus creating a mixed solution with a

dx.doi.org/10.1021/jp506259k | J. Phys. Chem. C 2014, 118, 20026−20033

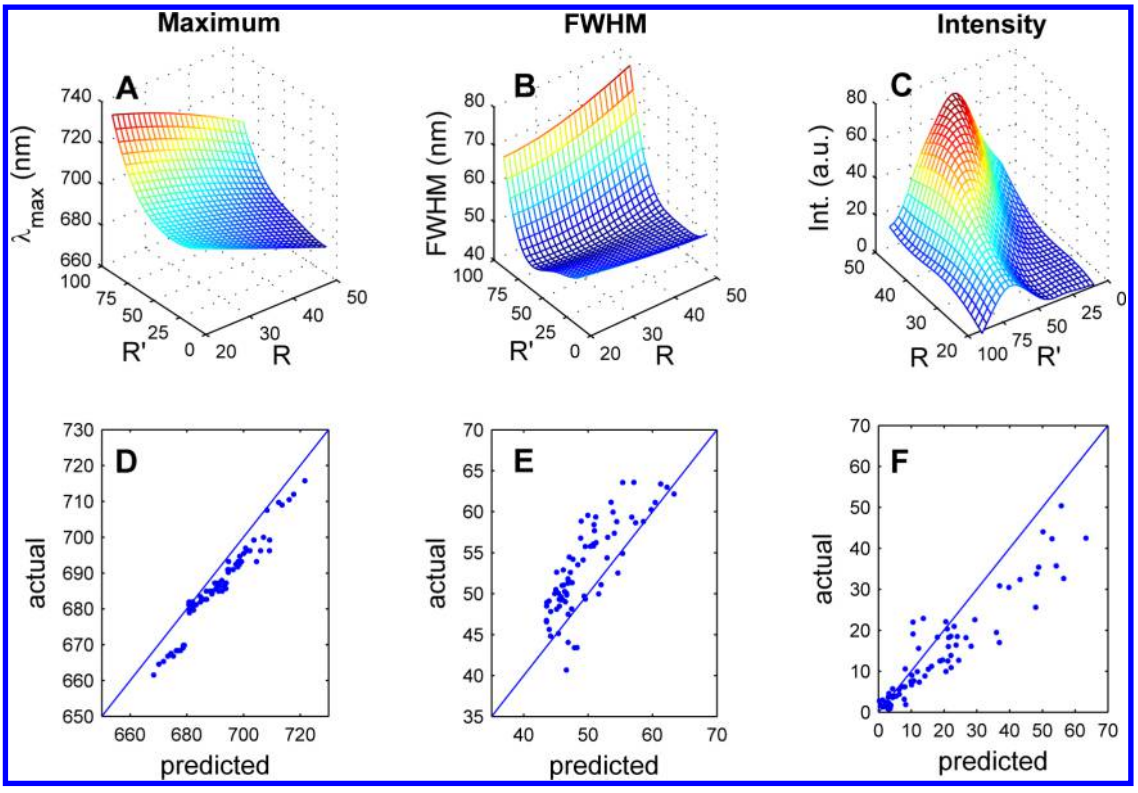

Figure 7. Metamodels for CdSeTe predicting luminescence maximum (A), fwhm (B), and intensity (C) for t fixed at 75 s. The model was evaluated by measuring 25 evenly distributed samples at t = 45, 75, and 105 s. The predicted vs actual plots for maximum (D), fwhm (E), and intensity (F) below the models contain all 75 validation samples.

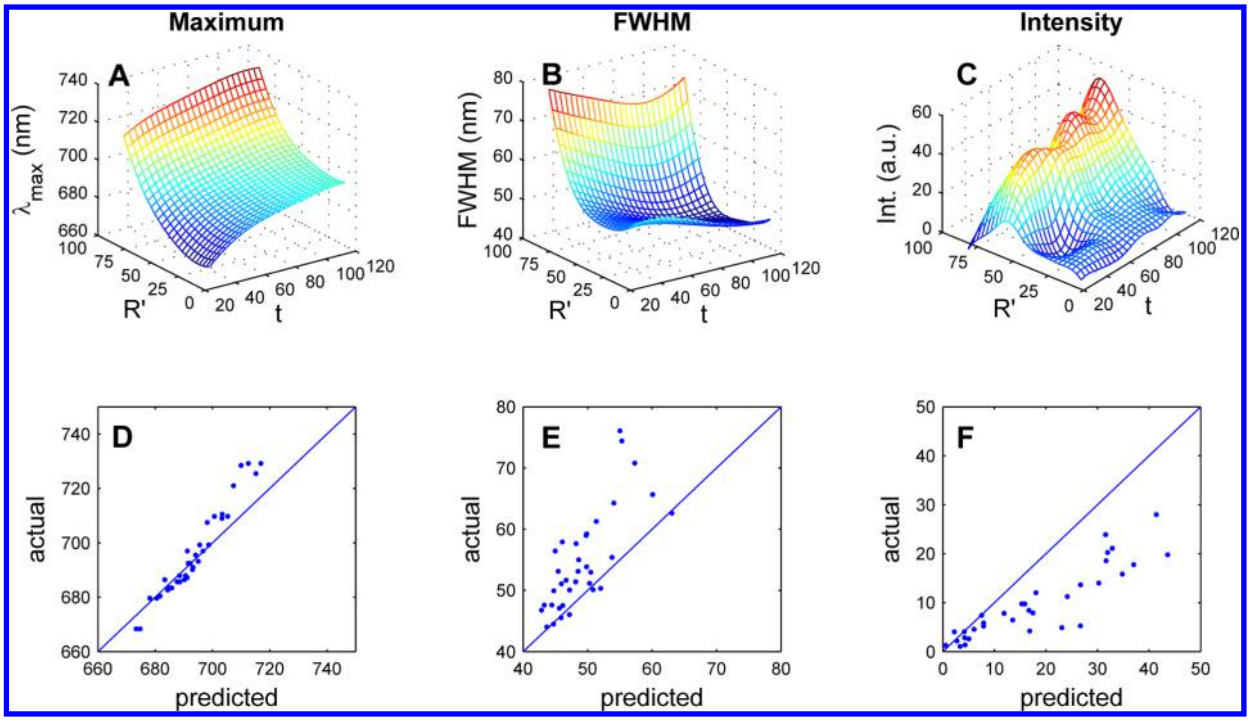

Figure 8. Metamodels for CdSeTe predicting luminescence maximum (A), fwhm (B), and intensity (C) for R fixed at 33. The model was evaluated by measuring 36 evenly distributed samples on the R = 33 surface and plotting actual vs predicted.

molar ratio of Se:Te of 1:1. The value of R was always maintained below 50 since at higher values parallel nucleation of CdSe is observed. Additional problems arise due to the lower solubility of the product particles which occasionally led to precipitation within the droplets. This precipitation causes some degree of reactor fouling. The time to reactor failure depends on a variety of parameters, such as Te-content of the precursor solution, temperature, and reaction time. In a typical experiment with randomized sampling the reactor would fail after approximately 120 measurements. Accordingly, including

dx.doi.org/10.1021/jp506259k | J. Phys. Chem. C 2014, 118, 20026−20033

a safety margin of about 20 measurements, the capillary was changed every 100 measurements to avoid blockage.

To represent and evaluate the data, surfaces with t fixed and variable R and R' are shown in Figure 7. The luminescence maximum shifts to lower energies as a function of both R and R'. The highest intensities and lowest fwhm are obtained when R' is approximately 50 whereas R is less influential. To validate the model, evenly distributed points on surfaces of fixed t were measured and compared to the prediction. The results for the luminescence maximum show high accuracy with a slight systematic error that is attributed to the need to change capillaries for the evaluation experiments. New capillaries are not completely stable and induce drifts as shown in Figure 4. Importantly, this drift does not appreciably affect the prediction if the measurements are made in a random fashion (e.g., using a Latin hypercube). In this case, however, the measurements for prediction and evaluation were taken one after another and with different capillaries. This introduces a systematic error. For fwhm measurements, the experimental values are above the prediction due to the precipitation problems. The trend in emission intensity is accurately predicted with deviations increasing as a function of intensity. The precipitation is dependent on further parameters not considered in the model, such as the speed of the droplets, the age of the capillary, and other hidden parameters.

Figure 8 shows the results for R fixed at 33. From the maximum model it is evident that R' has a higher influence than the reaction time. As expected the bandgap energy decreases with higher tellurium content. The fwhm has its lowest values around $R' = 50$ with the intensity being highest between $R' = 50$ and 75. The residence time is much less influential. The validation experiment with 36 evenly distributed points on the $R = 33$ surface demonstrates again much better performance for the prediction of the fluorescence maximum than for fwhm and intensity. However, general trends can still be clearly identified. The systematic error introduced by exchanging capillaries is present again. The deviation from the predicted values is partly attributable to the higher complexity of the reaction system but also on the presence of hidden parameters which will control the tendency of CdSeTe to aggregate and precipitate.

SUMMARY AND CONCLUSION

A stable and reliable reactor for the synthesis of semiconductor quantum dots (CdSe and CdSeTe) has been developed. The products exiting the reactor are monitored spectroscopically online, thus eliminating the need for sample collection. Recording of photoluminescence spectra and control of the syringe pumps to set new reaction conditions in terms of residence time, flow rate, and precursor ratios are fully automated. The collected spectra are analyzed with MATLAB to extract the characteristic parameters fwhm, fluorescence emission maximum and intensity. These values are then used as inputs for a metamodeling algorithm based on Universal Kriging. The model predicts the reactor output at arbitrary points within the chosen parameter space. The accuracy of the prediction has been demonstrated via the synthesis of colloidal semiconductor quantum dots with excellent results in the case of CdSe and good results for the ternary alloy CdSeTe.

The method presented above is fast, reliable, and accurate. No physical parameters for the reaction are needed as input thus rendering preliminary experiments redundant. This work is highly relevant for the field of colloidal quantum dot synthesis as the amounts needed for commercial applications are easily accessible via microfluidic methods.[34] Combining the method presented herein with a scaled out reactor will allow the commercial production of high-quality bespoke quantum dots with defined emission maximum. From a microfluidics point of view the approach is also of high value. It has been argued that the most important output of a microfluidic experiment is information.[37,38] Via Universal Kriging the information output of the experiment can be maximized without increasing the number of performed experiments.

ASSOCIATED CONTENT

Supporting Information

Shape functions to obtain the models for CdSe and CdSeTe, MATLAB code, and experimental data used to obtain the metamodel for CdSe. This material is available free of charge via the Internet at http://pubs.acs.org.

AUTHOR INFORMATION

Corresponding Author

*E-mail: Andrew.deMello@chem.ethz.ch.

Notes

The authors declare no competing financial interest.

ACKNOWLEDGMENTS

The authors would like to thank Professor J. C. deMello and Dr. A. M. Nightingale for helpful discussions. The authors also acknowledge Dr. Stavros Stavrakis for assistance with the spetroscopic detection system. This work was partially supported by the Swiss National Science Foundation grant (200021_143638).

REFERENCES

(1) Alivisatos, A. P. Semiconductor Clusters, Nanocrystals, and Quantum Dots. *Science* **1996**, *271*, 933−937.

(2) Rao, C. N. R.; Thomas, P. J.; Kulkarni, G. U. *Nanocrystals: Synthesis, Properties and Applications*; Springer Series in Materials Science; Springer: Duesseldorf, Germany, 2007; Vol. *95*.

(3) van Santen, R. A. Complementary Structure Sensitive and Insensitive Catalytic Relationships. *Acc. Chem. Res.* **2009**, *42*, 57−66.

(4) Aricò, A. S.; Bruce, P.; Scrosati, B.; Tarascon, J.-M.; van Schalkwijk, W. Nanostructured Materials for Advanced Energy Conversion and Storage Devices. *Nat. Mater.* **2005**, *4*, 366−377.

(5) Shirasaki, Y.; Supran, G. J.; Bawendi, M. G.; Bulović, V. Emergence of Colloidal Quantum-Dot Light-Emitting Technologies. *Nat. Photonics* **2013**, *7*, 13−23.

(6) Alivisatos, P. The Use of Nanocrystals in Biological Detection. *Nat. Biotechnol.* **2004**, *22*, 47−52.

(7) Lal, S.; Clare, S. E.; Halas, N. J. Nanoshell-Enabled Photothermal Cancer Therapy: Impending Clinical Impact. *Acc. Chem. Res.* **2008**, *41*, 1842−1851.

(8) Norris, D. J.; Nirmal, M.; Murray, C. B.; Sacra, A.; Bawendi, M. G. Size Dependent Optical Spectroscopy of II−VI Semiconductor Nanocrystallites (Quantum Dots). *Z. Phys. D* **1993**, *26*, 355−357.

(9) Murray, C. B.; Kagan, C. R.; Bawendi, M. G. Synthesis and Characterization of Monodisperse Nanocrystals and Close-Packed Nanocrystal Assemblies. *Annu. Rev. Mater. Sci.* **2000**, *30*, 545−610.

(10) Krishnadasan, S.; Brown, R. J. C.; deMello, A. J.; deMello, J. C. Intelligent Routes to the Controlled Synthesis of Nanoparticles. *Lab Chip* **2007**, *7*, 1434−1441.

(11) Edel, J. B.; Fortt, R.; deMello, J. C.; deMello, A. J. Microfluidic Routes to the Controlled Production of Nanoparticles. *Chem. Commun.* **2002**, 1136−1137.

(12) Elvira, K. S.; Casadevall i Solvas, X.; Wootton, R. C. R.; deMello, A. J. The Past, Present and Potential for Microfluidic Reactor Technology in Chemical Synthesis. *Nat. Chem.* **2013**, *5*, 905−915.

(13) Lignos, I.; Protesescu, L.; Stavrakis, S.; Piveteau, L.; Speirs, M. J.; Loi, M. A.; Kovalenko, M. V.; deMello, A. J. Facile Droplet-based Microfluidic Synthesis of Monodisperse IV−VI Semiconductor Nanocrystals with Coupled In-Line NIR Fluorescence Detection. *Chem. Mater.* **2014**, *26*, 2975−2982.
(14) Park, J.; Joo, J.; Kwon, S. G.; Jang, Y.; Hyeon, T. Synthesis of Monodisperse Spherical Nanocrystals. *Angew. Chem., Int. Ed.* **2007**, *46*, 4630−4660.
(15) Invitrogen, retrieved May 2014. http://www.lifetechnologies.com/ch/en/home/brands/molecular-probes/key-molecular-probes-products/qdot.html.
(16) Orimoto, Y.; Watanabe, K.; Yamashita, K.; Uehara, M.; Nakamura, H.; Furuya, T.; Maeda, H. Application of Artificial Neural Networks to Rapid Data Analysis in Combinatorial Nanoparticle Syntheses. *J. Phys. Chem. C* **2012**, *116*, 17885−17896.
(17) Chan, E. M.; Xu, C.; Mao, A. W.; Han, G.; Owen, J. S.; Cohen, B. E.; Milliron, D. J. Reproducible, High-Throughput Synthesis of Colloidal Nanocrystals for Optimization in Multidimensional Parameter Space. *Nano Lett.* **2010**, *10*, 1874−1885.
(18) Nakamura, H.; Yamaguchi, Y.; Miyazaki, M.; Maeda, H.; Uehara, M.; Mulvaney, P. Preparation of CdSe Nanocrystals in a Micro-Flow-Reactor. *Chem. Commun.* **2002**, 2844−2845.
(19) Chan, E. M.; Alivisatos, A. P.; Mathies, R. A. High-Temperature Microfluidic Synthesis of CdSe Nanocrystals in Nanoliter Droplets. *J. Am. Chem. Soc.* **2005**, *127*, 13854−13861.
(20) Shestopalov, I.; Tice, J. D.; Ismagilov, R. F. Multi-Step Synthesis of Nanoparticles Performed on Millisecond Time Scale in a Microfluidic Droplet-Based System. *Lab. Chip* **2004**, *4*, 316−321.
(21) Yen, B. K. H.; Stott, N. E.; Jensen, K. F.; Bawendi, M. G. A Continuous-Flow Microcapillary Reactor for the Preparation of a Size Series of CdSe Nanocrystals. *Adv. Mater.* **2003**, *15*, 1858−1862.
(22) Nightingale, A. M.; de Mello, J. C. Microscale Synthesis of Quantum Dots. *J. Mater. Chem.* **2010**, *20*, 8454−8463.
(23) Matheron, G. *Traité de Géostatistique Appliquée*; Technip: Paris, France, 1962; Vol. *14*.
(24) Cressie, N. A. *Statistics for Spatial Data*; Wiley (New York): Hoboken, NJ, 1993.
(25) Chiles, J.-P.; Delfiner, P. *Geostatistics: Modeling Spatial Uncertainty*, 2nd ed.; Wiley (New York): Hoboken, NJ, 2012.
(26) Cressie, N. The Origins of Kriging. *Math. Geol.* **1990**, *22*, 239−252.
(27) Mckay, M. D.; Beckman, R. J.; Conover, W. J. A Comparison of Three Methods for Selecting Values of Input Variables in the Analysis of Output From a Computer Code. *Technometrics* **2000**, *42*, 55−61.
(28) Koehler, J. R.; Owen, A. B. In *Computer Experiments*; Gosh, S., Rao, C. R., Eds.; Elsevier: Amsterdam, The Netherlands, 1996; Vol. *13*.
(29) Ye, K. Q. Orthogonal Column Latin Hypercubes and Their Application in Computer Experiments. *J. Am. Stat. Assoc.* **1998**, *93*, 1430−1439.
(30) Santner, T. J.; Williams, B. J.; Notz, W. I. *The Design and Analysis of Computer Experiments*; Springer (New York): Secausus, NJ, 2003.
(31) Jones, D. R.; Schonlau, M.; Welch, W. J. Efficient Global Optimization of Expensive Black−Box Functions. *J. Global Optim.* **1998**, *13*, 455−492.
(32) Eberly, S.; Swall, J.; Holland, D.; Cox, B.; Baldrige, E. *Developing Spatially Interpolated Surfaces and Estimating Uncertainty*; US Government Printing Office: Washington, DC, 2004.
(33) Kitanidis, P. K. Orthonormal Residuals in Geostatistics: Model Criticism and Parameter Estimation. *Math. Geol.* **1991**, *23*, 741−758.
(34) Nightingale, A. M.; Bannock, J. H.; Krishnadasan, S. H.; O'Mahony, F. T. F.; Haque, S. A.; Sloan, J.; Drury, C.; McIntyre, R.; deMello, J. C. Large-scale Synthesis of Nanocrystals in a Multichannel Droplet Reactor. *J. Mater. Chem. A* **2013**, *1*, 4067−4076.
(35) Gurusinghe, N. P.; Hewa-Kasakarage, N. N.; Zamkov, M. Composition-Tunable Properties of CdS_xTe_{1-x} Alloy Nanocrystals. *J. Phys. Chem. C* **2008**, *112*, 12795−12800.
(36) Bailey, R. E.; Nie, S. Alloyed Semiconductor Quantum Dots: Tuning the Optical Properties Without Changing the Particle Size. *J. Am. Chem. Soc.* **2003**, *125*, 7100−7106.
(37) Mitchell, M. C.; Spikmans, V.; Manz, A.; de Mello, A. J. Microchip-Based Synthesis and Total Analysis Systems (μSYNTAS): Chemical Microprocessing for Generation and Analysis of Compound Libraries. *J. Chem. Soc., Perkin Trans. 1* **2001**, 514−518.
(38) McMullen, J. P.; Stone, M. T.; Buchwald, S. L.; Jensen, K. F. An Integrated Microreactor System for Self-Optimization of a Heck Reaction: From Micro- to Mesoscale Flow Systems. *Angew. Chem.* **2010**, *122*, 7230−7234.